Effect of the local wall cooling/heating on the hypersonic boundary layer stability and transition

Andrey Sidorenko, Yury Gromyko, Dmitry Bountin, Pavel Polivanov and Anatoly Maslov

Khristianovich Institute of Theoretical and Applied Mechanics (ITAM)
Russian Academy of Science
RUSSIA 630090, Novosibirsk, Institutskaya str. 4/1

Abstract

Hypersonic boundary layer stability and transition were studied experimentally and numerically for the test case of 7°cone model with local wall heating and cooling. The experiments were performed for M=6, heat flux distributions and wall pressure pulsations were measured. It was obtained that variation of the wall temperature significantly affects the transition location. It was found that development of the second mode depends on the upstream wall temperature. The results of numerical simulation confirm the general trends of the second mode evolution obtained in the experiment.

1. Introduction

The development of secure and re-usable re-entry vehicle requires the complete control of the heat distribution on its thermal protection system (TPS). During the most critical re-entry phase, the hypersonic flow along the vehicle initiates a laminar boundary layer inside of which most of the transfer phenomena take place (heat, momentum and mass transfer). If at one position of the vehicle, this boundary layer experiences a transition from the laminar to the turbulent regime then at the corresponding position the TPS will receive a sharp increase of the incoming heat flux (minimum 3 times higher). If the vehicle aims to be re-usable, it is mandatory to protect it adequately against this overheat. Therefore aerospace designer needs to receive the proper information and tools allowing a better prediction and ultimately a better control of the transition in hypersonic regime.
For configurations having aerodynamically smooth surfaces, transition is associated with excitation in the boundary layer and downstream amplification of unstable modes, namely, the first and second modes [1-4]. Although features of these instabilities and opportunities of their control have been studied by the research community for more than fifty years, they have been focused on boundary layers having fairly uniform distributions of the wall temperature and heat fluxes [4-7]. However, actual TPS may have elements of different heat conductivity and/or emissivity. Junctures between these elements lead to jumps of the heat-transfer boundary conditions. Furthermore, active TPS may produce regions of localized relative heating or cooling of the aerodynamic surface. These thermal non-uniformities may significantly affect the boundary-layer mean flow, excitation and evolution of unstable modes and, ultimately, transition locus. Investigation of physical mechanisms associated with the foregoing thermal effects will help us to design advanced thermal protection systems providing capabilities of transition control.
An effect of local cooling / heating on the development of the boundary layer disturbances was studied numerically and experimentally in framework of FP7 project TransHyBeriAN for the test case of the hypersonic flow formed above the 7° cone under zero angle of attack.

2. Wind tunnel experiments

2.1 Experimental setup

The supersonic wind tunnel “Tranzit-M” (ITAM) is a short duration aerodynamic facility with range of Mach number M = 4 ÷ 8, and high values of Reynolds number. Scheme of the wind tunnel is presented in Fig 1. Initially the air is accumulated in the first prechamber and volumes of the ohmic heaters, where after heating it acquires high temperature and pressure. After opening of the high-speed valve, the gas is been throttling into the second prechamber and afterwards it is flowing into the test section through the contoured nozzle. Runtime of the wind tunnel is limited by the volume of the vacuum tank (6.5 m^3) and approximately equal to 110÷200 ms for M = 6. The

wind tunnel is equipped with pressure and temperature sensors in the first and second prechambers. The diameter of the contoured nozzle is 300 mm.

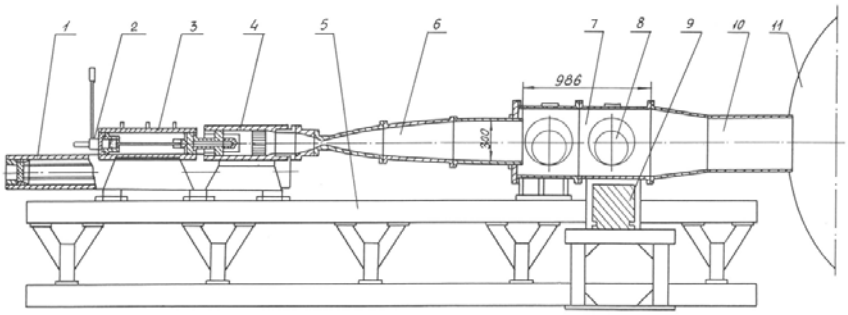

Figure 1 : Wind tunnel "Tranzit-M" (1 - ohmic heater, 2 – high-speed valve, 3 - first prechamber, 4 - second prechamber, 5 – frame, 6 - contoured nozzle, 7 -test section, 8 - optical windows, 9- isolated model base, 10 – diffuser, 11 - vacuum tank).

The experiments were carried out for M = 6, stagnation temperature $T_0 = 370$ K and the stagnation pressure $P_0 = 3.8 \div 12$ bar. Reynolds number has varied in range of $\mathrm{Re}_1 = (4 \div 20) \times 10^6$ m^{-1}. Figure 2 shows variation of the parameters P_0 и T_0 measured in the second prechamber during a run of the wind tunnel. It can be seen that after the opening of the fast valve there is a graduate change of stagnation parameters. For each run of the wind tunnel the data analysis was performed for time window where Re_1 was within 5%. The corresponding time window is shown in Figure 2. Depending on the initial flow parameters, the duration of the window was varied from 90 to 200 ms. The pressure and temperature data reading were averaged within the window to obtain P_0 and T_0 .

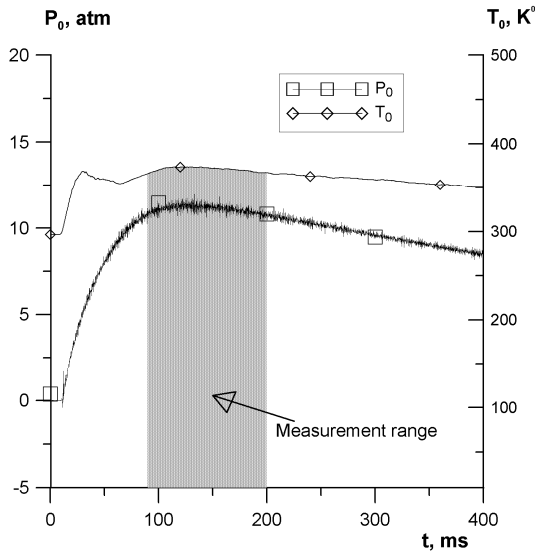

Figure 2 Stagnation pressure and temperature of the flow during a run

The experimental model to study an effect of the spatial temperature gradients on the boundary layer transition was a 7° - half angle cone with sharp nose. The drafts of the model are presented in Figure 3 and Figure 4. The model is assembled from 4 sections including the interchangeable cooler and heater sections. The cooler is made from copper and utilize liquid nitrogen flow to control the temperature. The heater has the same cowl and ceramic insert with ohmic heater inside. Typical time of operation to achieve the maximum/minimum temperature is about 120÷200 seconds. The main part of the model body is made from PEEK to prevent heat diffusion. The maximum temperature of the heater was dictated by PEEK properties and limited by $T_w = 440$K. Minimum temperature of the cooler was close to boiling point of liquid nitrogen ($T_w = 90$K) The model is equipped by pressure sensors PCB 132A31 to measure the pulsations of the surface pressure. Positions of the sensors are indicated in Figure 4. The spectra obtained by PCB 5 were used to set zero angle of attack and sideslip of the model.

Pressure sensors were used with a signal converter PCB Piezotronocs 482S05. The data were recorded by means of ADC L-card E20-10 with sampling frequency 2 MHz. Intrinsic noise of pressure sensors were measured before each experiment and taken into account in processing of data.

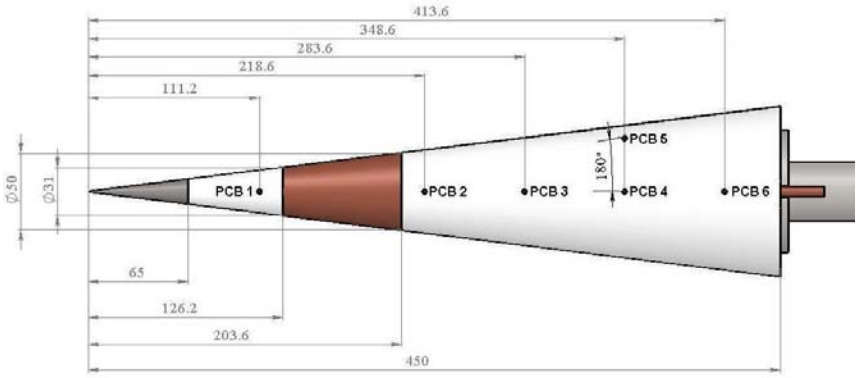

Figure 3 Draft of the 7-degree cone model and positions of pressure sensors.

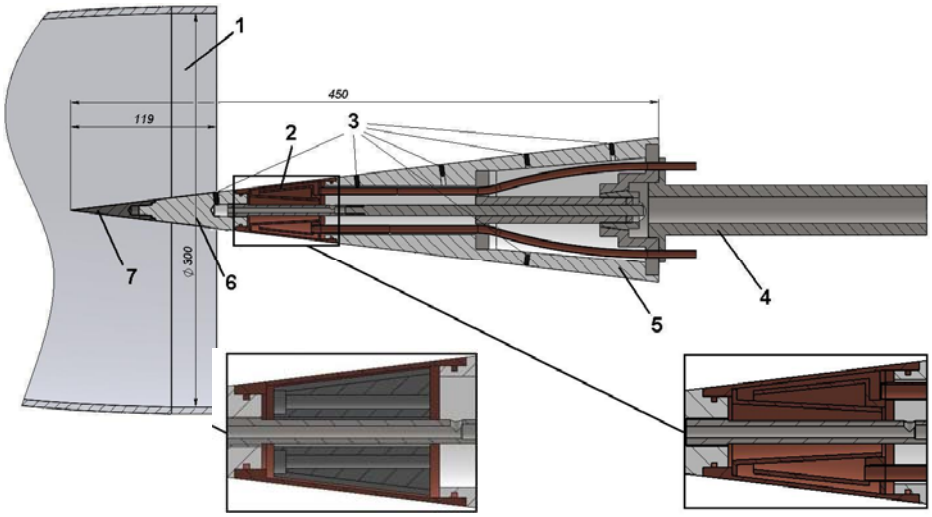

Figure 4 Draft of the model with heater/cooler sections (1-wind tunnel nozzle; 2 - heater/cooler section; 3- PCB sensor; 4- model support; 5- flare section; 6- middle section; nose section).

Spectral analysis of the pressure pulsation was performed by the discrete Fourier transform. Spectral distributions were calculated by averaging over L blocks on 2^n samples in each block. Usually the number of blocks was varied from 428 to 858, with the number of samples in the block 1024 and 512, respectively. The spectra obtained were used for calculation of the mean-square level of fluctuations in a given frequency band.

Additionally to pressure pulsation measurements the transition location was investigated by IR technique. IR camera SVIT was used to measure distribution of temperature on the model surface during a run. The heat flux distributions were obtained from the surface temperature using assumption of semi-infinite body. Schlieren visualization was performed to detect density gradients in the flow hear the cooler/heater and to obtain intermittency level in the transitional boundary layer. High speed camera Phantom 310m was used with frame rate 8.6 kHz.

2.2 Experimental results

In the experiments the cone model was initially under room conditions (T = 290K) and the temperature distribution was uniform everywhere. After vacuumization of the test chamber the desired temperature of the cooler/heater T_w was achieved and the flow was started as soon as possible. Due to relatively short time of T_w establishment and low heat conductivity of PEEK the region of the heat penetration was short enough. The wall temperature distributions measured right before the run of the wind tunnel are presented in Figure 5.

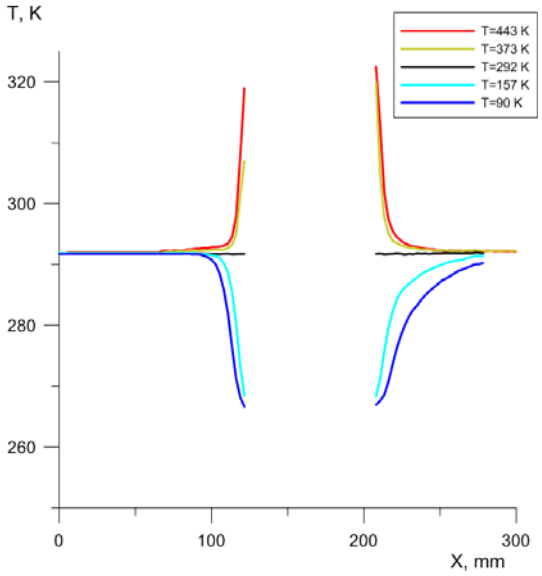

Figure 5 Wall temperature distributions at the moment of the test for various T_w

Below the experimental results are presented as the summarized data for the cases of reference conditions, heating and cooling of the surface section. The experiments were performed for Reynolds number from 4.2 to 20×10^6 m^{-1} and each run was repeated twice.

Schlieren visualization was performed to study the flow in vicinity of the cooler/heater and to detect the turbulent spots in transitional boundary layer. The averaged Schlieren images of the flow above the heated and cooled surface elements are presented in Figure 6. The knife edge orientation was horizontal in these experiments so one can see the corresponding density gradients. The shock wave is followed by expansion waves in the case of heater. The flow pattern is reversed in the case of cooler.

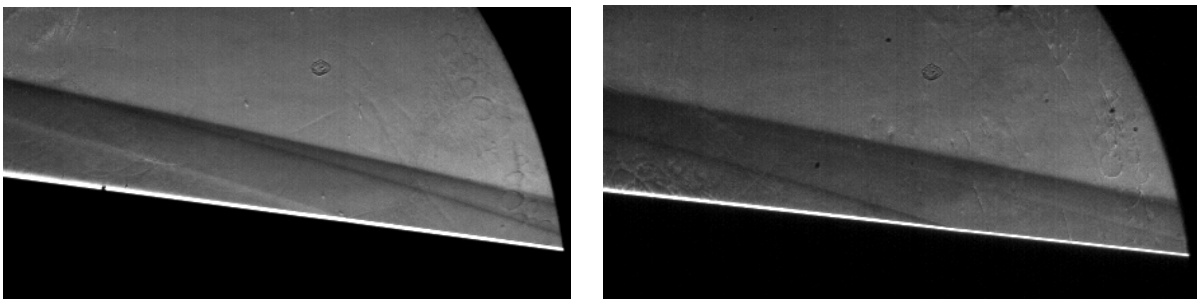

a) b)

Figure 6 Schlieren visualization of the flow near the heater/cooler (flow from the right to the left): a – heating (T_w = 440 K); b – cooling (T_w = 90 K).

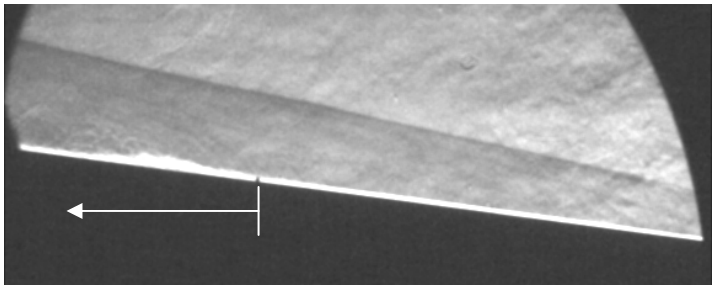

Figure 7 Turbulent spot on the Schlieren visualization.

Turbulent spots were detected in the instantaneous schlieren images as zones of the boundary layer inflation (Figure 7). The positions of the inflation beginning was defined for each frame of and presented in Figure 8. The curves in the figures present filtered data to reveal the general trend. Running average filter was used with window of 150 samples. It can be seen that heating effectively shifts transition beginning upstream and cooling shifts it downstream.

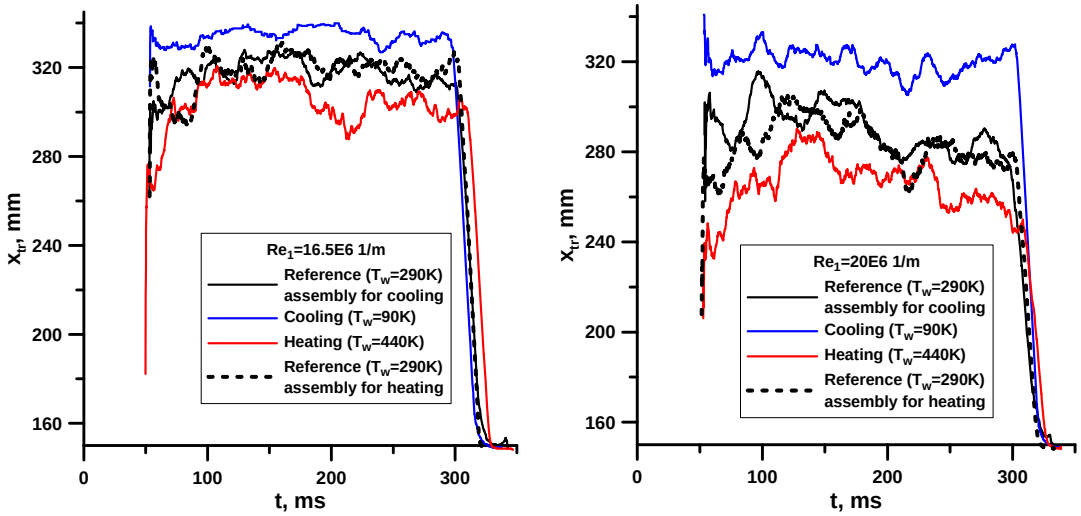

Figure 8 Transition beginning position obtained from Schlieren visualization.

Intermittency levels based on Schlieren visualization are presented in Figure 9. It is necessary to take into account that the intermittency is defined as ratio of number of frames where the transition was detected upstream of the point to the total number of frames. It can be seen that the surface cooling intensively delays the transition. The effect of the heating is opposite and less pronounced.

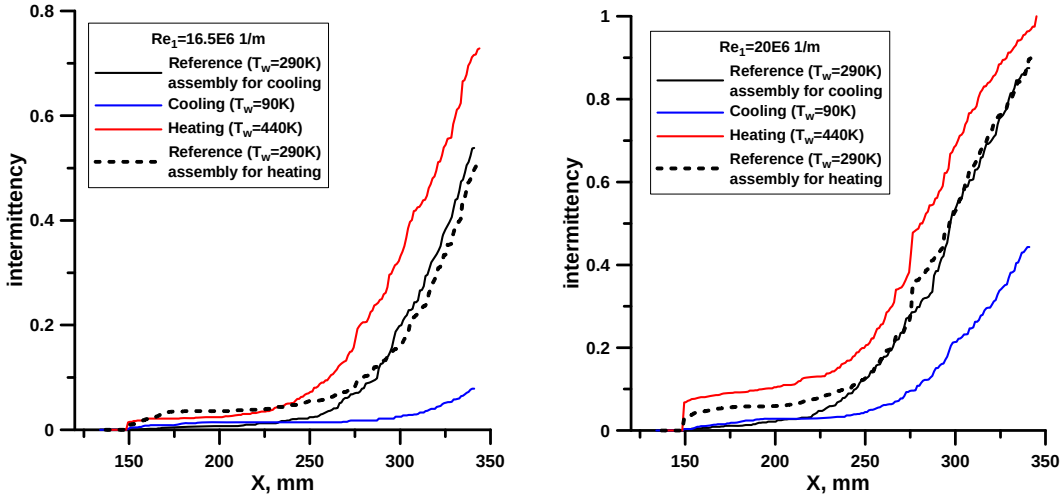

Figure 10 Intermittency in the transitional boundary layer.

Heat flux distributions were measured by IR camera for various Re and temperature factors of the surface section. The data are summarized in the Figure 11 as streamwise distributions of Stanton number. The data are presented for the region downstream of the heater/cooler. The Stanton number was calculated as: $St = Q/(\mathrm{Re}_{1e}\mu_e C_p(T_0-T_{surf}))$, where Q - the measured value of the heat flux.

It can be seen from the Figure 11a that for low Re the boundary layer is mostly laminar and the heat flux is nearly constant for the reference test case. The curves for heated and cooled surface element reveal the heat exchange of the surface with the boundary layer heated or cooled upstream. The heat accumulated in BL during its passage above the heater increases the heat flux to the model body downstream. The heat flux downstream of the cooler is accordingly lower than the reference values. This effect is evident in all figures.

It is commonly accepted that maximum of the heat flux (or Stanton number) is associated with the end of transition and increasing of the heat flux corresponds to transitional boundary layer. This maximum may be found for the first time in the case of heating for $\mathrm{Re}_1=8.3\times10^6 \mathrm{m}^{-1}$. At the same time there is no evident maximum for the reference and cooling cases at this Reynolds number. Increasing of Re results in movement transition location upstream and transition end may be clearly seen in the following figures.

The general effect of local surface temperature is shown in the Figure 11 (a-e). Cooling of the surface effectively shifts the transition location downstream and the magnitude of the effect size depends on temperature factor T_w/T_r .

Heating of the surface results in transition displacement upstream and this effect is less pronounced. It is necessary to take into account that maximum heating of the surface allowed to achieve the temperature factor $T_w/T_r = 1.4$. The positions of transition end obtained from the heat flux distributions are summarized in Figure 11e.

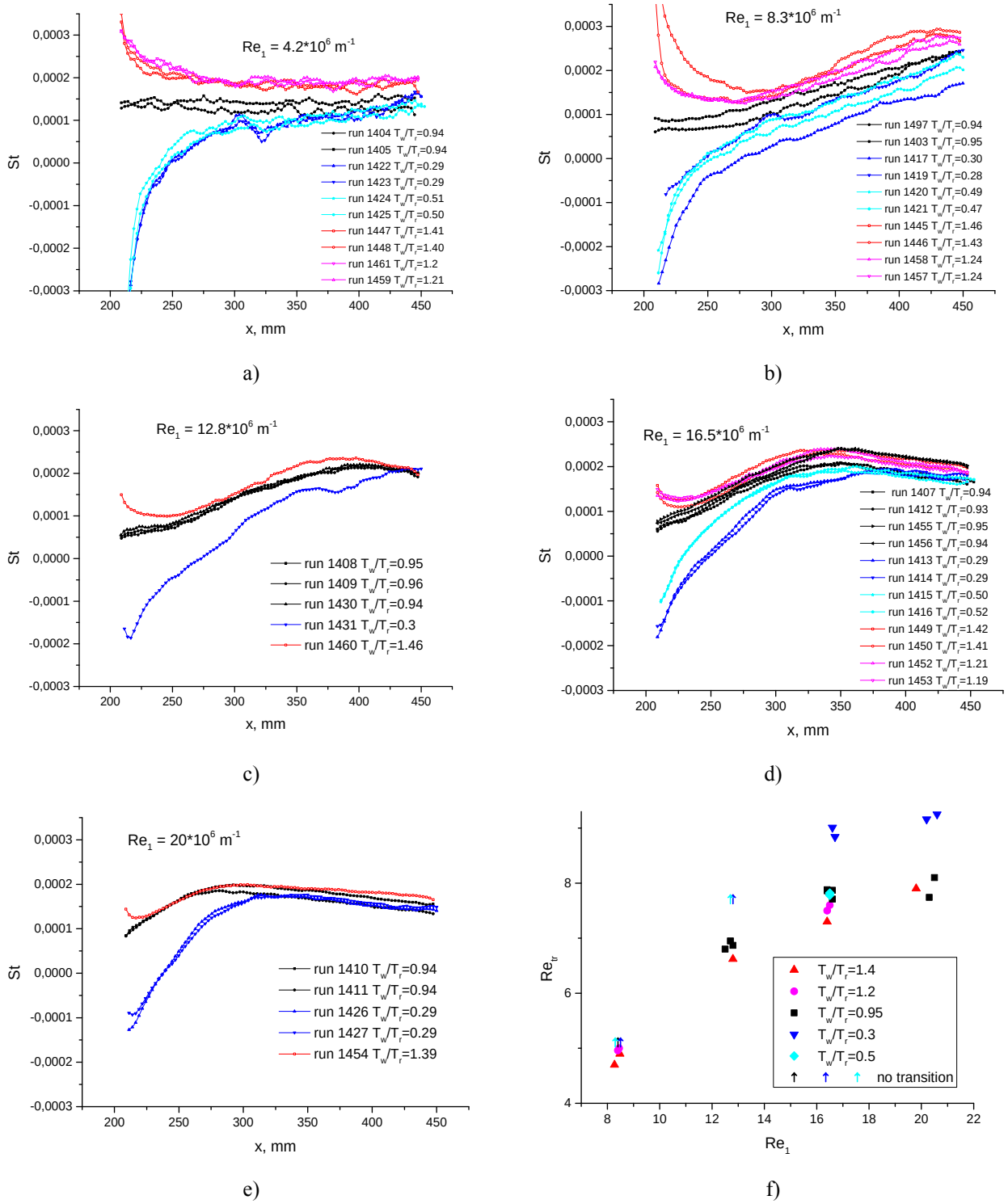

Figure 11 Distributions of Stanton number on the cone surface (a - e) and position of the transition end (f) for various Re_1.

Surface pressure pulsations were measured by means of 6 sensors. Five of them were placed in-line and used to study development of the disturbances in the boundary layer. Positions of the sensors are indicated in Figure 3. An example of the data obtained is presented in the following Figure 12 and Figure 13. These figures demonstrate variation of

spectra for two stations and various T_w/T_r with Reynolds number and comparison of pulsation spectra for various T_w/T_r at the same location. The data are presented as amplitude spectra of the pressure pulsations P' normalized by mean surface pressure P_e.

The evolution of the second mode with variation of Re_1 for the reference test case may be clearly seen in Figure 12a. At the station of PCB 2 the second mode amplitude is rising with increasing Re_1 and its frequency becomes higher due to decreasing of δ. At the downstream position of PCB 4 (Figure 12b) the gradual amplification of the second mode with Re_1 is broken by beginning of turbulization at $Re_1 = 8.36\times10^6$ m^{-1}. The spectra for higher Re_1 demonstrate decreasing of the second mode and filling of the spectra.

Cooling of the surface results in damping of the second mode and delay of its amplification as shown in Figure 12c and Figure 12d. Amplitude of the second mode for PCB 2 is much lower here. The transition at Figure 12d is also shifted to higher Re_1 in comparison with the reference case (Figure 12b).

Effect of the surface heating is shown in Figure 12e and Figure 12f for PCB 2 and PCB 4 correspondingly. It may be seen from the figures that pulsations of the second mode may be distinguished with amplitudes smaller than corresponding reference values. The shape of spectra shows that beginning of transition was found at PCB 2 for high Re_1. Analysis of Figure 12f reveals that the end of transition occurs at PCB 4 for $Re_1 = 16.6\times10^6$ m^{-1}.

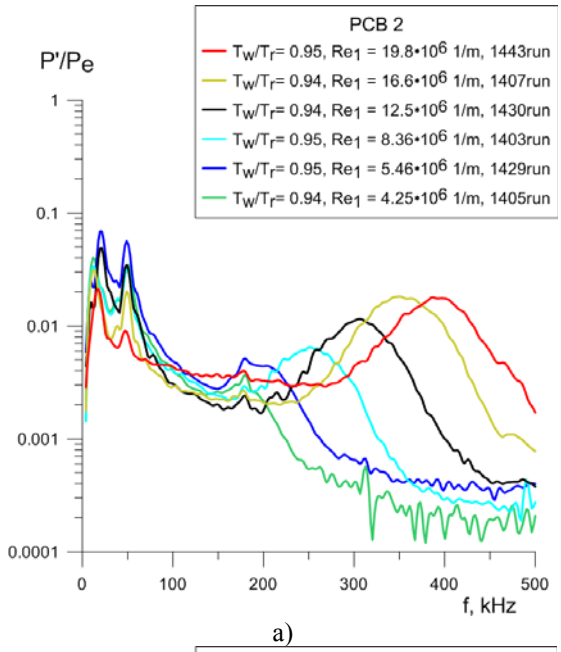

a)

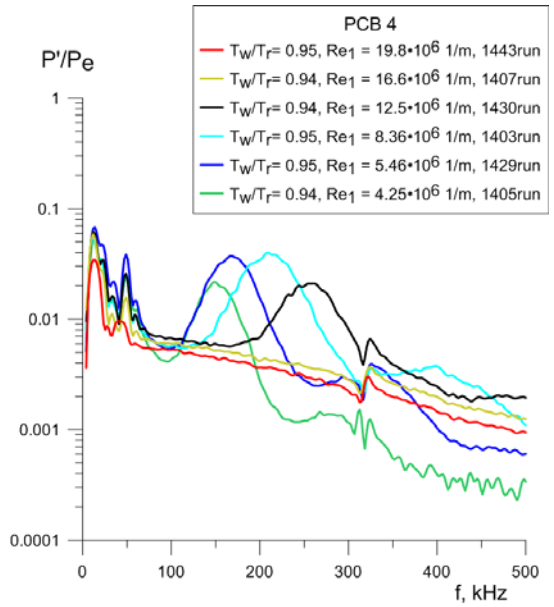

b)

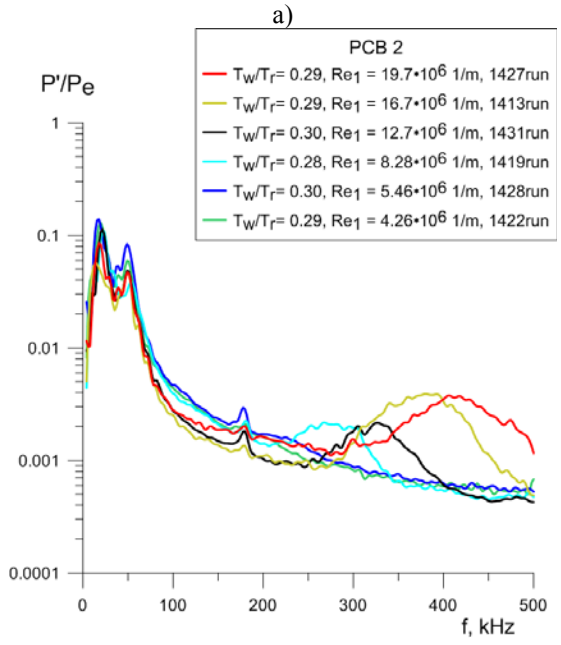

c)

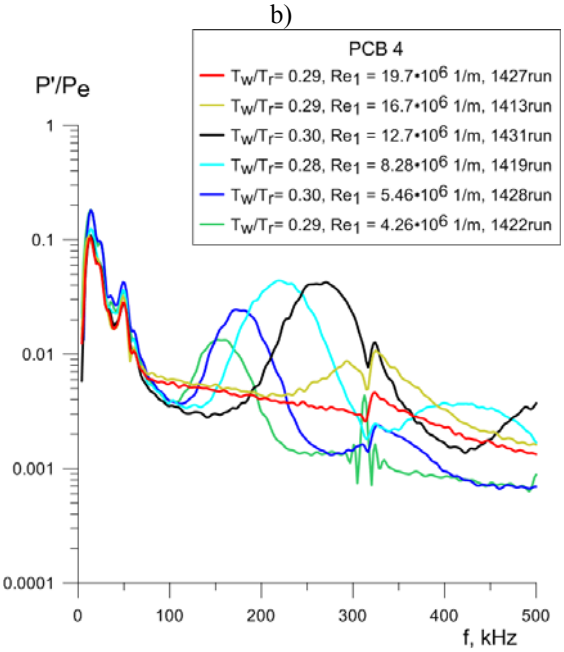

d)

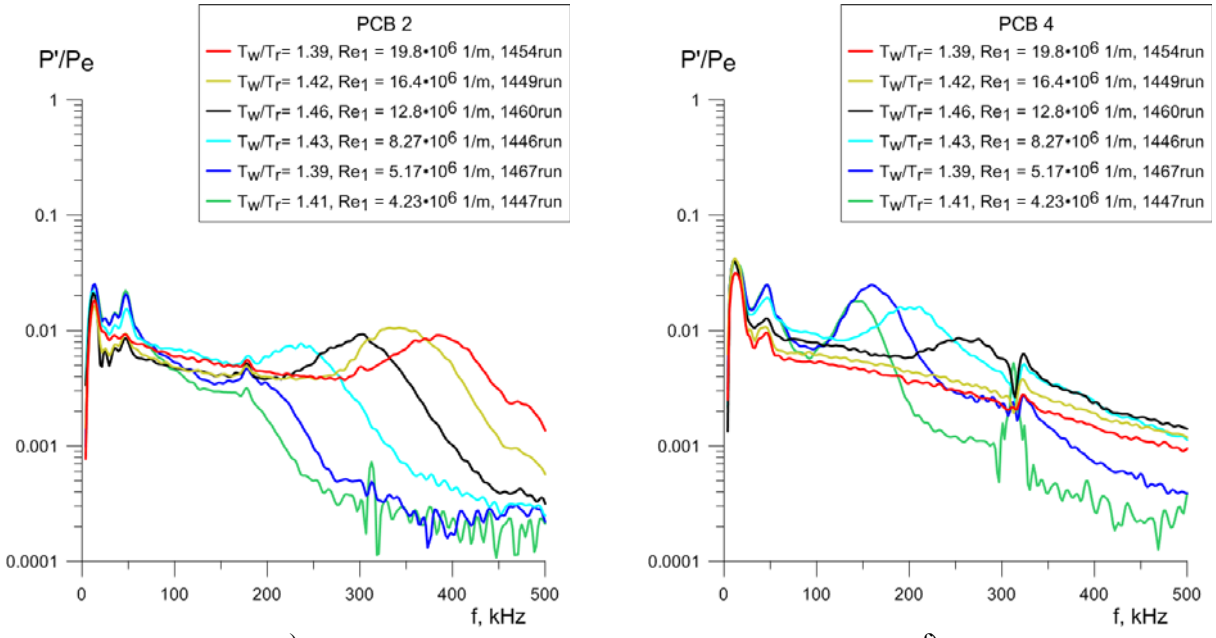

e) f)

Figure 12 Variation of pressure pulsation spectra for two stations and various *Tw/Tr* with Reynolds number.

Dependance of the pressure pulsation spectra on T_w/T_r for single sensor may be found in Figure 13. It may be seen for example from Figure 13b that the surface temperature affects the peak frequency of the second mode due to effect of the boundary layer thickness. The spectra corresponding to low Re_1 (Figure 13 a and b) show that cooling of the surface decreases amplitude of the second mode in laminar boundary layer. It is necessary to mention that second mode peak for the test case of heating is also decreased. It may be explained by beginning of nonlinear evolution of the second mode and dissipation of energy of pulsations. Increasing of the pulsation amplitude in range 80÷120 KHz supports this conclusion. It may be seen that with gradual increase of Reynolds number the nonlinear stage of disturbance development (Figure 13c and d) comes earlier for higher temperature factor, resulting in dissipation of the second mode and filling of the spectra. Transition end also comes earlier for high temperature factor as shown in Figure 13e. The spectra presented here reveal that the boundary layer is completely turbulent for all temperature factors except T_w/T_r = 0.39 where one can see the late stage of transition. Figure 13f shows completely turbulent boundary layer for all test cases.

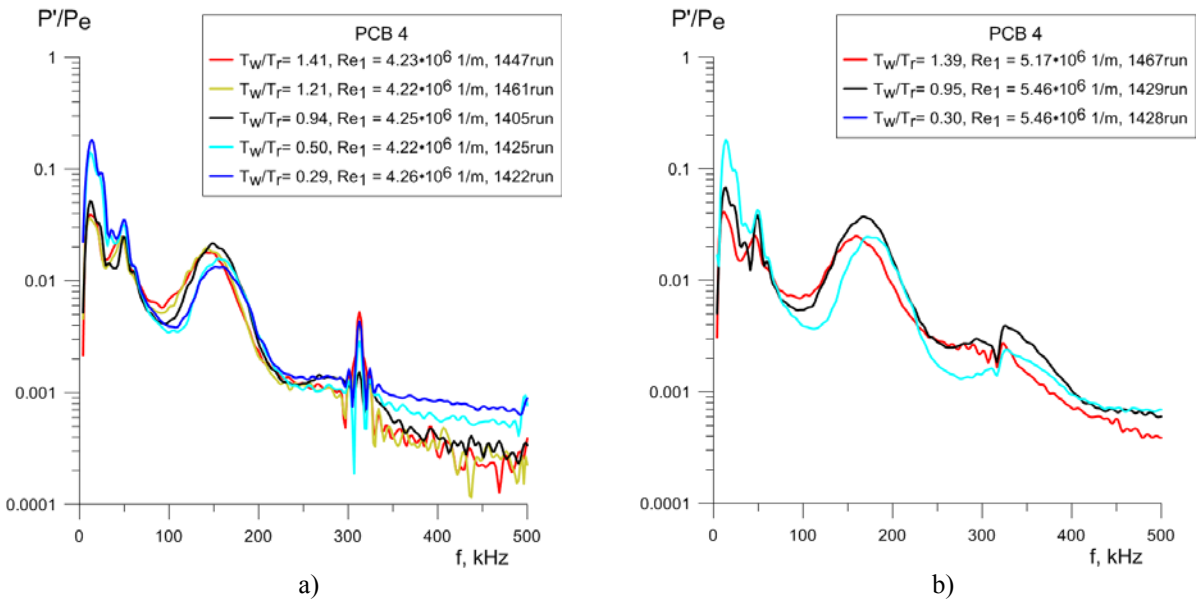

a) b)

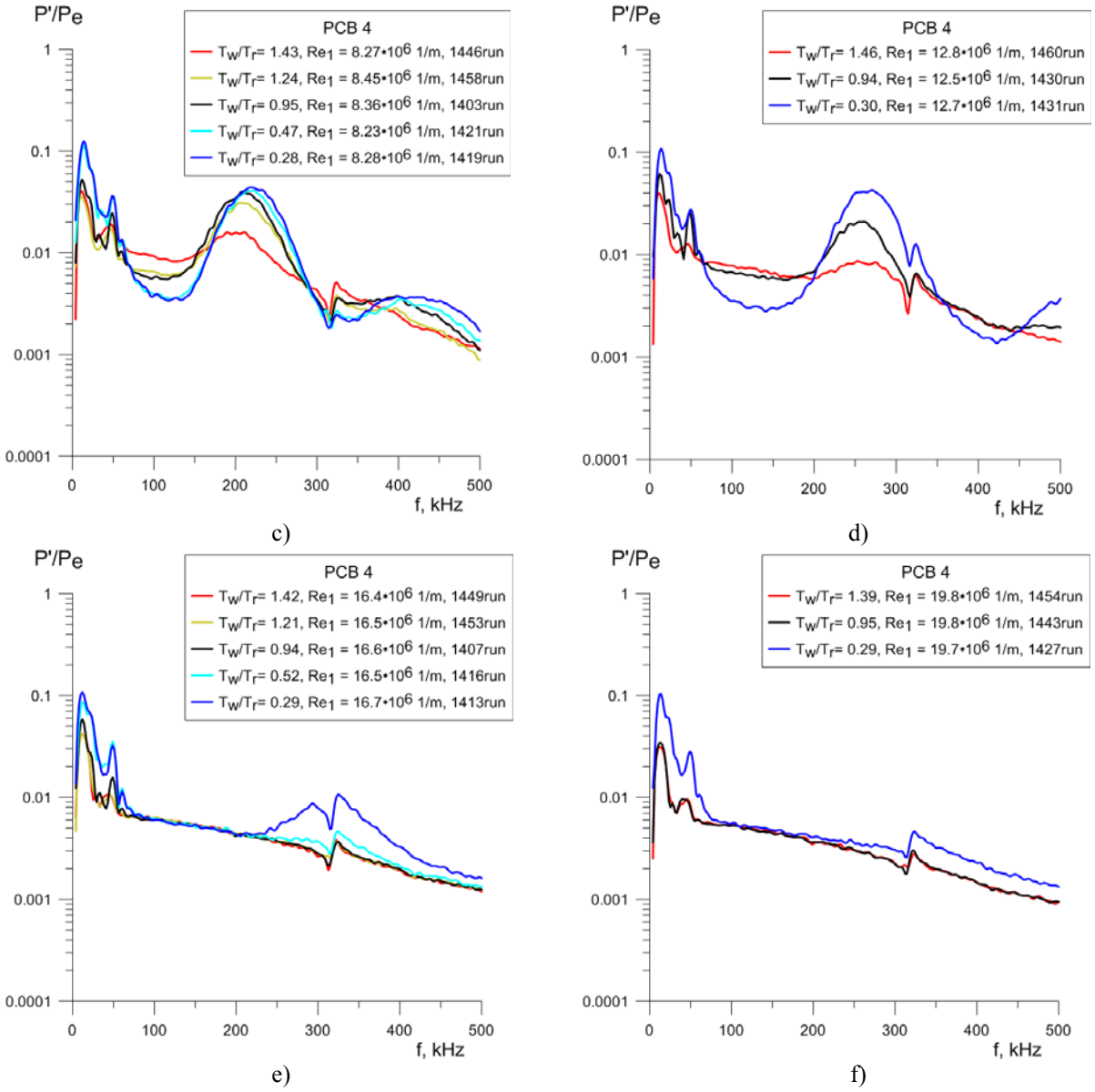

Figure 13 Comparison of the pressure pulsation spectra for various T_w/T_r at the same location.

3. Numerical simulation

The numerical simulation was performed for preliminary estimation of the experimental conditions and posterior analysis of the experimental data. Reliable modeling of laminar\turbulent transition is possible only by DNS and involves considerable computational power therefore it can not be used for the parametrical study. The current simulation deals only with linear stage of the disturbance development so the computations may be considerably simplified. The boundary layer stability was numerically studied in 2D assumption to simulate only development of the most unstable 2D waves of the second mode.

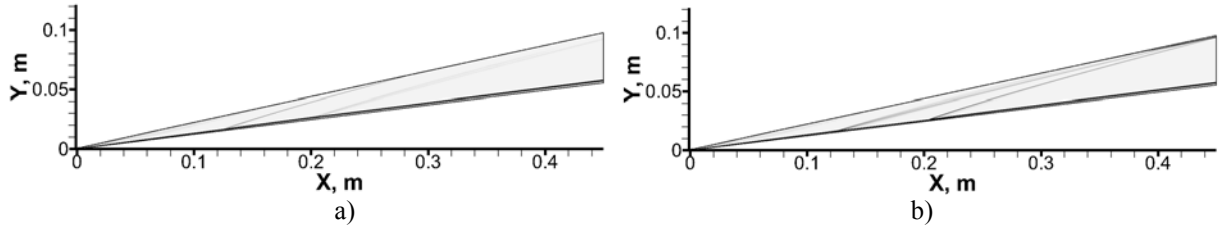

Figure 14 Spatial gradient of density: a) $T_w/T_r = 1.42$; b) $T_w/T_r = 0.26$.

The numerical simulation was performed only for $Re_1 = 5.75\times10^6$ m^{-1}. Commercial CFD software Fluent/ANSYS was used for simulation of axisymmetrical flow on the cone. Quadrilateral grid of 271×7500 cells was used for computations. The boundary layer conditions on the wall corresponded to the experimental ones. Three test cases were considered corresponding to reference conditions ($T_w = 293$K), local wall heating ($T_w = 450$K) and cooling ($T_w = 90$K). The temperature of the rest of wall was 293K. The gradient of the wall temperature on the cooler/heater border in simulation was sharp in comparison to the experiment (see Figure 5). The special study was done to study the effect of the wall temperature gradient of the disturbance development. It was found that small length of the heat penetration obtained in the experiment do not influence on the disturbance development. The CFD density gradients corresponding to the heated and cooled wall section are presented in Figure 14.

Generation of disturbances in CFD simulation was carried out by means of small synthetic jet on the model surface located at $x = 7$ mm. Sequential analysis of many frequencies is not efficient because the growth of perturbations occurs in a wide range of frequencies and separate review of a large number of discrete frequencies requires a substantial amount of computation time. Therefore it was decided to use linear combination of several harmonic waves of equal amplitude in frequency range $75 < f < 425$ kHz as the initial perturbation. An example of resulting synthetic disturbance is shown in Figure 15 where 18 waves are linearly combined. The preliminary calculations have shown a good agreement between the level of perturbation obtained in batch mode and reconstructed as sum of the individual frequencies. The disturbance spectra obtained in CFD simulation were normalized by spectrum of free flow pulsations obtained in the experiment and presented in Figure 15 (right panel) to take into account spectral content of the wind tunnel noise.

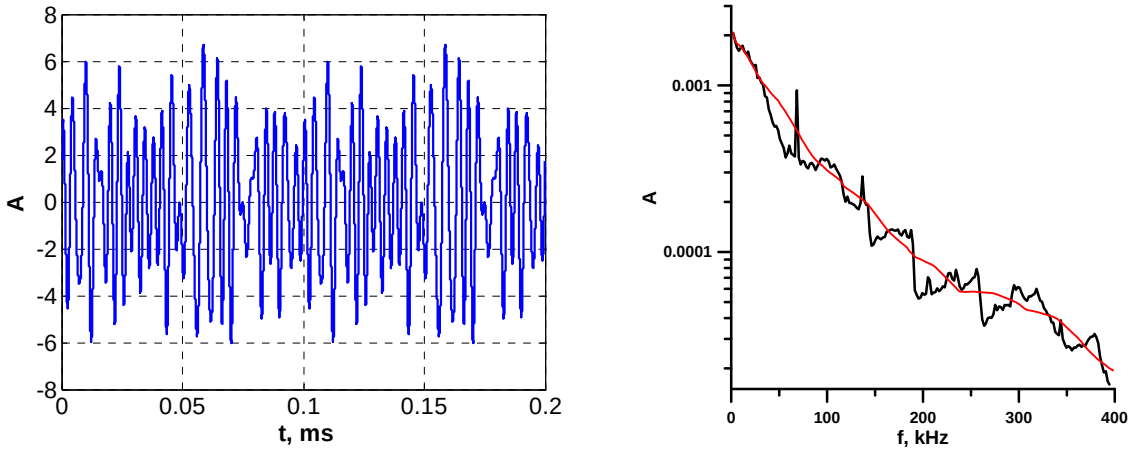

Figure 15 a) Iinitial synthetic disturbance; b) amplitude of wind tunnel noise,

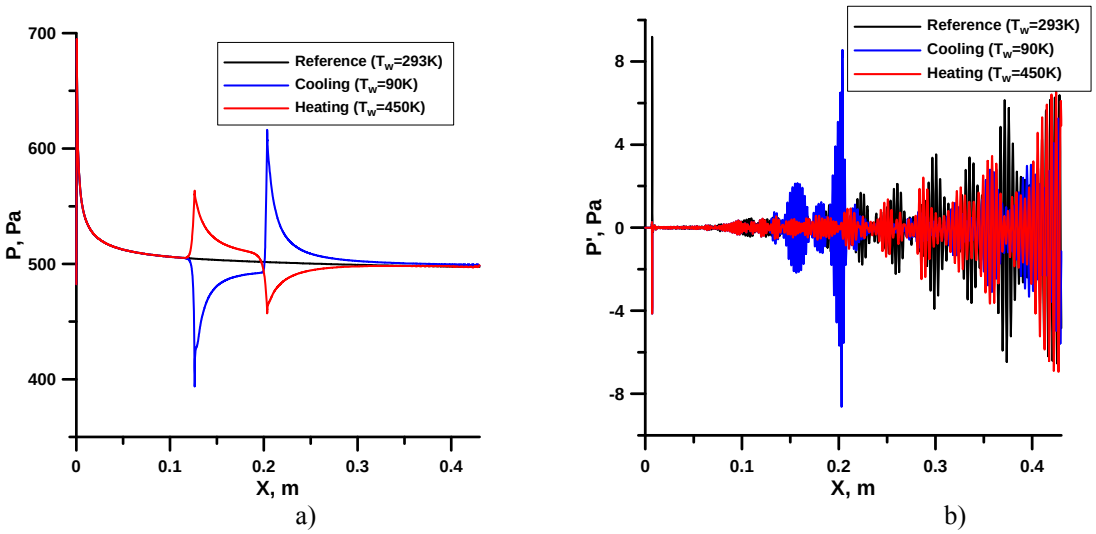

Figure 16 a) Mean surface pressure distribution; b) instantaneous value of surface pressure pulsations.

The distributions of mean surface pressure and instantaneous pressure pulsations are shown in Figure 16. It may be seen that the surface pressure gradients are higher in the case of cooling due to big difference in temperature factor in this case (T_w/T_r = 1.42 for heating and T_w/T_r = 0.26 for cooling). The effect of local surface cooling on the disturbance amplitude is very powerful but local as shown in the figure. Behind of the cooler the wave packed weakens and undergoes gradual growth further downstream. It has to be taken into account that the synthetic jet excites in the boundary layer a complex wave structure consisting from combination of many waves. Therefore the instantaneous pressure distributions reveal the beating as shown in Figure 16 (right).
The streamwise distributions of the pressure pulsation amplitude of the separated waves obtained by spectral analysis of the wave packet are presented in Figure 17. It may be seen that behaviour of the waves is strongly depending on their frequency. In comparison with the reference case the wave of the second mode with f = 150 kHz experiences higher amplification downstream of the heated surface section. The same wave behind the cooled wall section undergoes some delay of amplification (Figure 17a). There is no evident effect on this wave directly at position of the cooler/heater. In all test cases the wave is gradually amplified up to the right border of the domain.

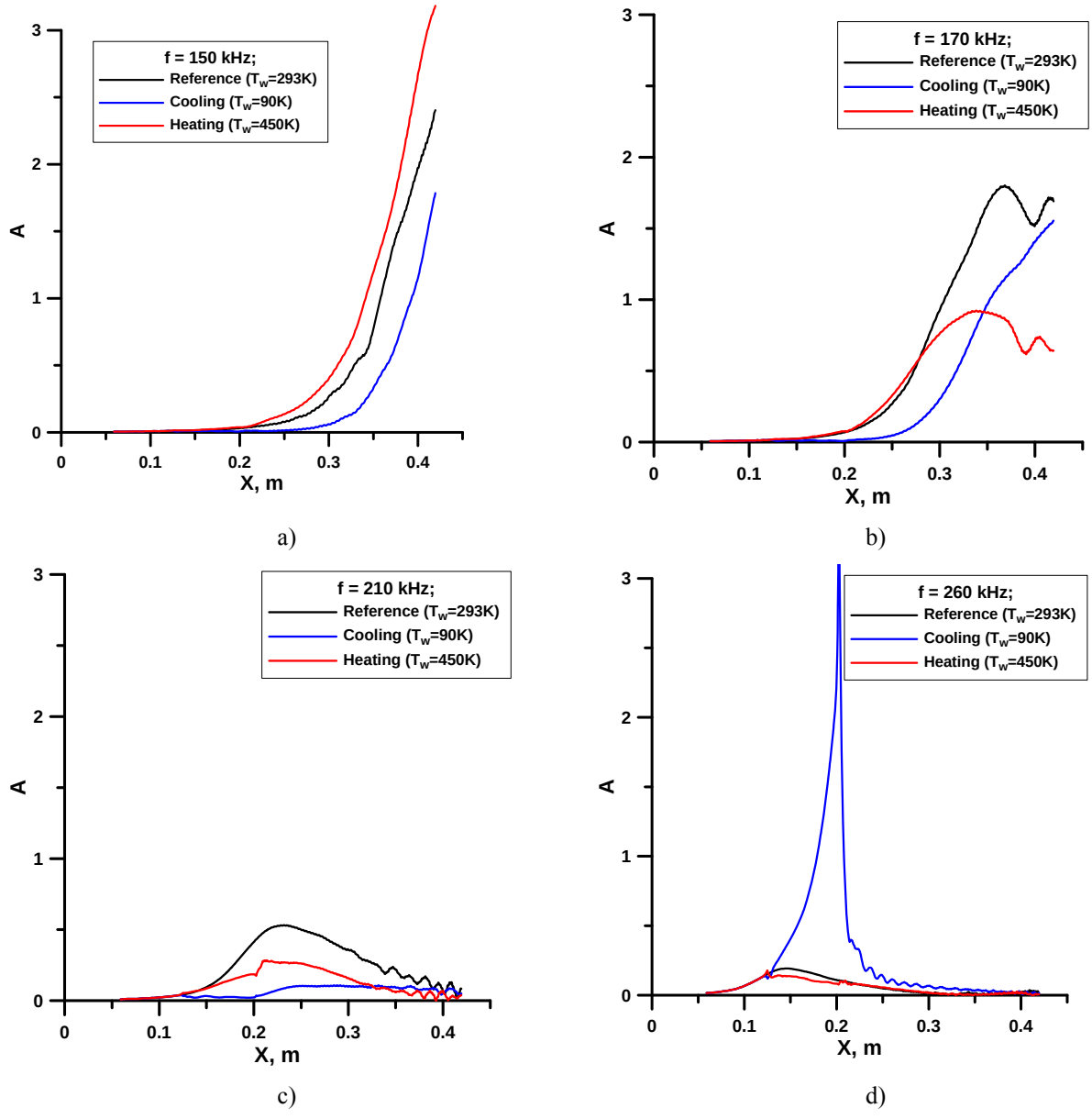

Figure 17 Streamwise distributions of amplitudes of isolated waves.

The wave of frequency 170 kHz demonstrates the same behaviour directly behind the heater/cooler (Figure 17b). Due to higher frequency this wave undergoes maximum amplification within the computational domain and begins to decay at $x = 0.37$ for the reference case. Due to expansion of the boundary layer above the heater and downstream the wave reaches its maximum faster and maximum amplitude is lower than in the reference case. In the case of cooling the boundary layer is thinner and growth of the wave is delayed.
The wave of higher frequency 210 kHz undergoes amplification and decay within the computation domain for all test cases (Figure 17c). The effect of local wall heating and cooling here is also associated with the change of the boundary layer thickness and profile downstream of the control section. The general effect of the temperature factor is the same and the resulting maximum amplitudes are much lower due to shorter region of amplification. This wave begins to amplify during its passage over the heater so some rise of the amplitude may be found at the heater boundary.
The wave of the highest frequency presented here corresponds to $f = 260$ kHz. This wave undergoes amplification upstream of the surface control section and its behaviour in the region of the cooler/heater may be seen from the Figure 17d. Upstream of the control section curves for all test cases coincide. The most evident effect presented in the figure in strong amplification of the wave in the region of the cooler. This amplification is explained by increasing of instability of the second mode waves on cold walls. Directly downstream of the cold wall section the wave is damped.

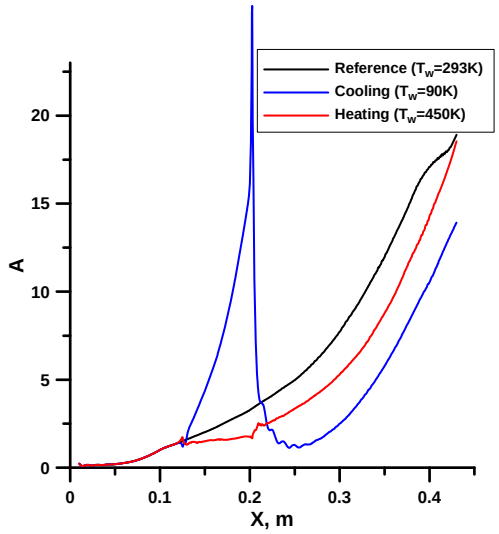

Figure 18 Streamwise distributions of RMS value of pressure pulsations

Streamwise distributions of RMS value of pressure pulsations are shown in Figure 18 for all CFD test cases. These values were obtained by recording of the wall pressures during considerable time period and include contribution of all frequencies of the wave packet. It may be seen from the figure that strong local amplification of some frequencies increase RMS value of the pressure pulsations above the cooler. Downstream of the cooler these waves rapidly decay and do not influence on RMS value of pulsations which is produced mostly by unstable waves of lower frequencies. Their behaviour determines the streamwise distribution of the RMS value of pulsations. It can be seen that for cooling and heating of the surface the RMS values are lower than in the reference case.
Figure 19 shows comparison of the pressure pulsation spectra measured in the experiment and obtained by CFD. The computational spectra were normalized by spectrum of free flow pulsations presented in Figure 15b. The initial amplitude of the wave packet in simulation was chosen to fit with the spectrum obtained by PCB 1 in the reference case.
The computational data are presented for positions of PCB 2,3,4 an 6 in comparison with corresponding experimental results. It can be seen from Figure 19 that there is good agreement of frequency of the second mode almost everywhere along the model between computations and the experiment. The agreement of the amplitude is also rather good taking into account experimental accuracy. It can be seen from the Figure 19b that cooling of the surface significantly reduces amplitude of the second mode at $x = 284$ mm. The amplitude for the case of heating is also less than in the reference case. Further downstream (Figure 19c) the disturbances of the second mode for all cases are amplified and amplification is higher for the case of cooling. Nevertheless the value of amplitude of the second mode for the case of cooling is lower than for other cases. Basing on these data we may conclude that local surface cooling significantly delays growth of the second mode. The second mode amplitude at position $x = 414$ mm for cooling is also much lower than reference value but the peak for heating is slightly higher.

It may be concluded that numerical simulation demonstrates very good agreement with the experimental data in terms of all details of the second mode development everywhere except the most downstream position. The experimental spectra demonstrate here slowdown of the second mode amplification for the reference and heating test cases. This effect is probably associated with early stages of the boundary layer transition.

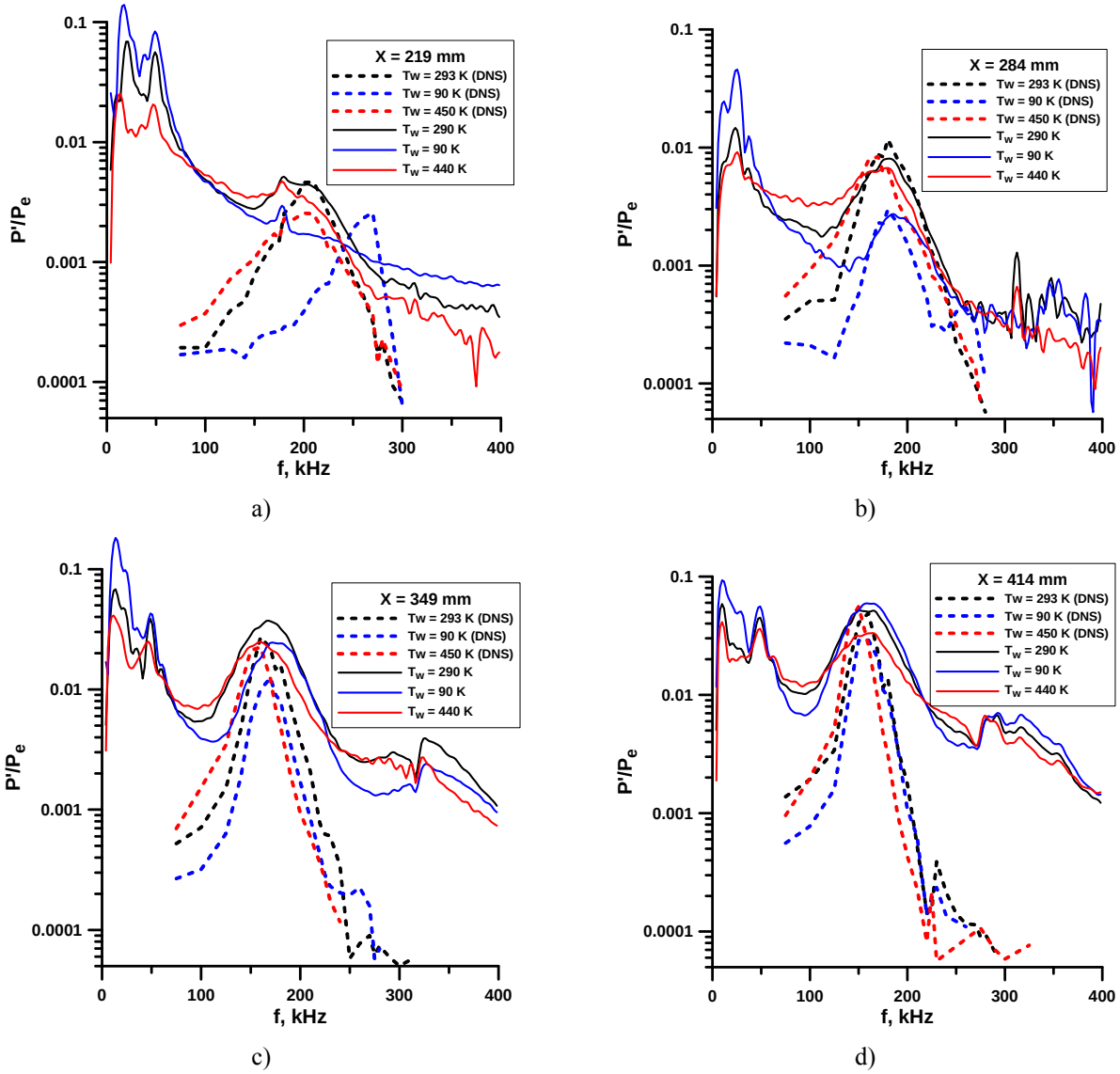

Figure 19 Comparison of pressure pulsation spectra

Conclusions

The experimental study of local surface temperature effect on the hypersonic boundary layer transition was performed for M=6 in wind tunnel «Tranzit-M». The boundary layer transition location was obtained by several techniques and development of the disturbances in the boundary layer was studied basing on unsteady surface pressure measurements. The experiments were performed in range of temperature factor $0.3< T_w/T_r = 1.4$ for wide range of Reynolds number.

It was obtained that the local surface temperature has strong effect on the boundary layer stability and transition. The experiments revealed that heating of the surface section accelerates the transition of the boundary layer downstream. Cooling of the surface element significantly delays the transition.

Development of the disturbances in the boundary layer was studied by means of the wall pressure pulsation measurement. It was obtained that wall temperature significantly affects the evolution of the second mode changing

its frequency and amplitude. It was shown that the second mode is damped by local wall cooling for low Reynolds number. Due to extended region of the boundary layer transition the results obtainned for higher Re are more complex and difficult to analize. Additional data processing have to be performed to study the wave packet development in the internittency region.
The numerical simulation was performed to study evolution of the wave packet in the boundary layer for experimental flow conditions. The numerical simulation demonstrates very good agreement with the experimental data in terms of all details of the second mode development.

Acknowledgements

The study was supported by EU in framework of TransHyBerAN FP7 project and RFBR (grant 12-01-00840-a)

References

[1] Malik, M.R., Zang, T.A., and Bushnell, D.M., Boundary Layer Transition in Hypersonic Flows. AIAA Paper No. 90-5232, 1990.
[2] Mack, L.M., Boundary-layer linear stability theory. AGARD Rep. 709 1984 (Special course on stability and transition of laminar flows).
[3] Malik, M.R., Prediction and Control of Transition in Supersonic and Hypersonic boundary Layers. *AIAA J.,* Vol. 27, No. 11, 1989, pp. 1487-1493.
[4] Stetson, K.F., and Kimmel, R.L., On Hypersonic Boundary-Layer Transition. AIAA-92-0737, 1992.
[5] Anatoly A. Maslov, Alexander N. Shipyluk, Dmitry A. Bountin, and Andrey A. Sidorenko. Mach 6 Boundary-Layer Stability Experiments on Sharp and Blunt Cones. *Journal of Spacecraft and Rockets* 2006 43:1, pp.71-76.
[6] A. A. Maslov, A. V. Fedorov, D. A. Bountin, A. N. Shiplyuk, A. A. Sidorenko, N. D. Malmuth, and H. Knauss. Experimental Study of Disturbances in Transitional and Turbulent Hypersonic Boundary Layers. *AIAA Journal* 2008 46:7, pp.1880-1883
[7] Schneider, S.P., Hypersonic Laminar-Turbulent Transition on Circular Cones and Scramjet Forebodies. *Progress in Aerospace Sciences*, Vol. 40, 2004.